Optical and Quantum Electronics (2021) 53:439
https://doi.org/10.1007/s11082-021-03088-3

Highly sensitive plasmonic temperature sensor based on Fano resonances in MIM waveguide coupled with defective oval resonator

Ahlam Harhouz[1] · **Abdesselam Hocini**[1]

Received: 22 December 2020 / Accepted: 16 June 2021

Abstract
High sensitivity and a large detection range with simple design are highly desirable to realize temperature sensor. A highly sensitive temperature sensor based on Fano resonances in metal-insulator-metal (MIM) waveguide with Nano-wall side-coupled to oval resonator is proposed in this work. The Fano resonance is originated from the coherent coupling and interference between the discrete and the continua state. It shows a different profile, which is typically asymmetric and sharp line, in comparison with the Lorentzian resonance profile. The transmission properties are numerically simulated by finite-difference time-domain method. Structural parameters have a key role in the sensor's sensitivity and transmission spectrum that are studied to systematically analyze the sensing characteristics of such structure. The results of our study indicate that there exist Four-fano resonance peaks in the transmission spectrum. All of which has a linear relationship with the refractive index of the analyte under sensing. Through the optimization of structural parameters, sensitivity of 2.463 nm/°C is achieved, indicating the designed sensor can pave the way in the nano-integrated plasmonic devices for high-accurate temperature detection.

Keywords Fano resonance · plasmonic temperature sensor · metal-insulator-metal (MIM) waveguide · FDTD · RI sensor

1 Introduction

Surface plasmons polaritons (SPPs) are electromagnetic waves that trap on metal-dielectric interface (MacDonald et al. 2009; Barnes et al. 2003; Barnes et al. 2003) , which has the capability to overcome the typical diffraction limit and is regarded as an intriguing field optical manipulation (Zayats et al. 2005), control, processing (Yin et al. 2012; Zhou et al. 2015; Ozbay 2006) , sensing (Liu et al. 2010; Hocini et al. 2021; Yan et al. 2015; Achi et al. 2020), and nano integrating (Barnes et al. 2003).

✉ Ahlam Harhouz
ahlam.harhouz@univ-msila.dz

[1] Laboratoire d'Analyse des Signaux et Systèmes, Department of Electronics, University of M'Sila, P.O.BOX.166, 28000 Route Ichbilia, M'Sila, Algeria

Published online: 22 July 2021

In recent years, surface wave-based sensing techniques like Bloch surface wave (BSW) and surface plasmon (SPR) have been used in a variety of bio-sensing applications due to their inherent advantages, such as immune to electromagnetic interference, rapid response time, real-time and label-free detection.(Goyal and Saini 2020; Wang et al. 2017; Bashiri et al. 2019; Goyal and Pal 2020) Plasmonic sensing has been an important research field and has been widely used in detecting trace molecules in biology and chemistry (Liu et al. 2010; Yan et al. 2015; Achi et al. 2020; Tong et al. 2014) . To date, many plasmonic designs based on SPPs have been proposed to realize sensors with high performance of detection. These devices are based on MIM waveguides and made up of waveguides coupled with resonators. Due to the good properties of light confinement (Wen et al. 2014; Yu et al. 2019) , wide available frequency range, the absence of bending loss and easy to manufacture, sensors based on MIM plasmonic waveguides have aroused a great interest (Achi et al. 2020; Wang et al. 2019; Hocini et al. 2020; Ghorbani et al. 2018) . furthermore, MIM waveguide coupled resonators can produce special optical effects, such as Fano resonance (Wen et al. 2014; Piao et al. 2011; Yu et al. 2015) and in some cases, electromagnetically induced transparency (EIT) (Piao et al. 2012). Fano resonance exhibits a sharp asymmetric line-shape deriving from the interference between a discrete state and a wide continuum state, providing high figure of merit (FOM) in measurements (Wen et al. 2014; Ghorbani et al. 2018) . Compared to the symmetric Lorentzian characteristic line-shape supported by the LSPR of MNPs , plasmonic systems based on Fano resonance are likely to be highly sensitive sensors due to their useful properties such as asymmetric line-shape, hight confinement to the nanometer scale, strong electromagnetic field enhancement, (Chen et al. 2015; Wen et al. 2015). The reduction of the levels of transmittance spectrum from peak to trough is easily achieved. The full wide half magnitude (FWHM) of this transmittance spectrum is relatively slender, can easily be identified, and tracked resulting in significant enhancement in the sensing resolution (Binfeng et al. 2016).

Due to the useful properties of the Fano resonance, recently, a group of researchers have used Fano resonance for temperature sensing (Kong et al. 2016; Chatterjee et al. 2019; Chen et al. 2019; Lin et al. 2019) , where the sensing performance depends on sharper spectral configuration; which leads to higher figure of merit (FOM) to provide high-accurate and robust measurement.

In order to acquire miniature plasmonic temperature sensor with high sensitivity and FOM, a nanoscale Fano resonance based device composed of coupled plasmonic MIM waveguide is proposed in this study. The sensor is composed of MIM waveguide with Nano-wall side-coupled to oval resonator. Four fano resonances can be generated based on this design. The Fano resonances are investigated with different ethanol temperatures infiltred in the oval resonator, Peak transmittance, the resonant wavelength and line width can also be tuned by the geometric parameters. Certified by numerical simulation based on the finite-difference time-domain (FDTD) method, the optimized plasmonic temperature sensor gives sensitivity greater than 0.44 nm/°C with high figure of merit FOM that is competitive with the reported sensors.

2 Prototype design and simulation method

The plasmonic structure based on Fano resonance is schematically shown in Fig. 1a, it consists of a defective oval resonator and a MIM waveguide with a thin metal nano-wall directly below the oval resonator. Three rectangular silver grooves (Fig. 1b) with width

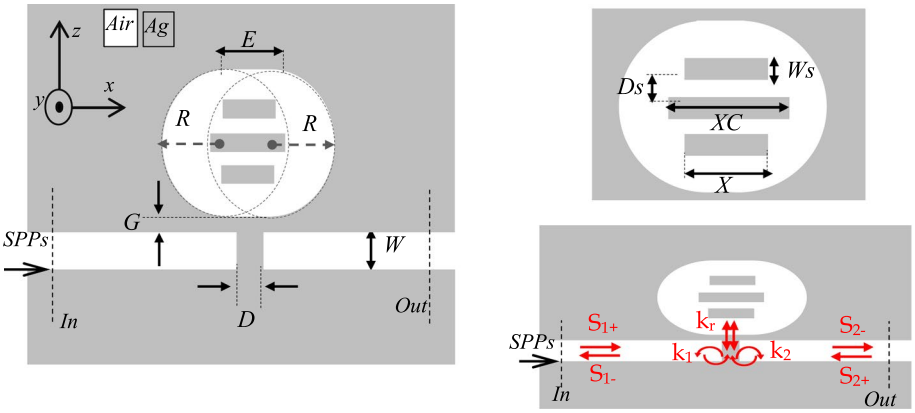

Fig. 1 **a** the proposed design. **b** The zoomed defective cavity. **c** analytic equivalent model for CMT .The geometrical parameters of the proposed structure were set as $w = 50$ nm, $D = 50$ nm, $R = 300$ nm, $G = 10$ nm, $E = 60$ nm, $Ws = 60$ nm, $Ds = 60$ nm, XC = 300 nm, $X = 250$ nm

(Ws) and length (XC, X) are inserted into the oval resonator to generate a defect, and their positions are described by the distance (Ds). To ensure that only the fundamental TM0 type SPPs mode can be excited and transmitted, the width of MIM waveguide is fixed as $w = 50$ nm throughout this work (Gai et al. 2007), and the thickness of the nano-wall is D. The MIM waveguide is coupled with a side oval resonator above the nano-wall, with R as radius of two disks intertwined with distance (E). The gray and white areas represent the silver layer and the dielectric material respectively. Due to the lower ohmic loss, the metal in the model (Silver) is selected as material whose relative permittivity can be described by the Drude model (Lu et al. 2011; Zhang et al. 2016a; Dong et al. 2018) :

$$\varepsilon_m(\omega) = \varepsilon_\infty - \frac{\omega_p^2)}{\omega(\omega + i\gamma)} \tag{1}$$

where ε_∞ is the dielectric constant at the infinite angular frequency with a value of 3.7, ω is frequency of incident wave,$\omega_p = 1.38 * 10^{16} Hz$ is the bulk plasma frequency, and $\gamma = 2.73 * 10^{13} Hz$ is the electron collision frequency.

In our simulation scenario, the transmission characteristics of the MIM waveguides coupled with nano- wall and oval cavities are simulated by FDTD using the commercial simulator R-Soft. The propose topology in this paper is 2D for which the 2D FDTD has been used, that is to say, along the y direction the structure is supposed to be infinite. However, in reality the structure has to have a finite height. In a previous study (Danaie and Shahzadi 2019) the 2D and 3D results have been compared to different values of height along the y direction. This study has shown that 2D structures , such as our case, when the structure's length along the y axis increases, the 3D results tend to the 2D results. The Perfectly Matched Layers (PMLs) is utilized to simulate the top and bottom boundaries of the structure. The uniform mesh grid (Δx,Δz) equal to 5 nm was chosen in both the x and z directions (Bensalah et al. 2019) to ensure the speed and the accuracy of the calculation. The source is Gaussian light, placed on the left side of the waveguide. Once the incident light is TM-polarized wave, the SPPs will be excited, confined and transmitted in the MIM waveguide. The MIM waveguides coupled with the nano-wall and oval cavity are analyzed

based on the temporal coupled-mode theory (CMT) (Li et al. 2010). To clarify the Fano resonance phenomena, certain parameters are introduced in Fig.1c, namely, the SPP wave of the cavity (S_i, S_t) and the coupling coefficients between the input waveguide and the nano-wall cavity (k_1), between the output MIM waveguide and the nano-wall cavity (k_2), and between the nano-wall cavity and defective oval cavity (k_r) . When a certain optical wave with ω frequency is launched on the input port of the MIM waveguide, transmittance T can be calculated as follows (Piao et al. 2011; Tang et al. 2017) :

$$T = \left|\frac{s_t}{s_i}\right|^2 = \frac{k_1 k_2 [j(\omega - \omega_r) + k_r^2]}{[j(\omega - \omega_s) + k_1^2 + k_2^2 + k_r^2][j(\omega - \omega_r) + k_r^2] - k_r^2}|^2 \quad (2)$$

where ω_s and ω_r are the resonance frequencies of the nano-wall and oval cavities.

2.1 Analysis and discussion

In this section, the numerical results due to the interaction of the incident waves with our designed sensor are presented. In order to comprehend the effect of an inserted nano-wall side-coupled to defective oval resonator on the waveguide, the simulated transmission spectra are numerically calculated by FDTD method and given in Fig. 2a. here the geometrical parameters of the proposed structure were set as $w = 50$ nm, $D = 50$ nm, $R = 300$ nm, $G = 10$ nm, $E = 60$ nm, $Ws = 60$ nm, $Ds = 60$ nm, $XC = 300$ nm, $X = 250$ nm. The green curve (Fig. 2a) shows the transmission spectra of the simple MIM waveguide, it is greater than 0.8 in the range of 600–2500 nm. The transmittance of the waveguide with a metal nano-wall (black curve) is less than 0.16 in the same previous range. Obviously, the nano-wall will practically block the transmission and the spectrum can be seen as a wide continuum state. The red curve shows the transmission spectra of the waveguide with defective oval cavity, it is shown four sharp dips in the transmittance, of which the very narrow transmission valleys can be regarded as four discrete states. Once the nano-wall is inserted into MIM waveguide and coupled with defective oval resonator, the destructive interference between the one continuum state and the aforementioned four discrete states will happen, thus, four sharp and asymmetric Fano resonances will appear in the transmission spectrum. as indicated by the bleu curve in Fig. 2a, in which the Fano resonant peaks are respectively marked by FR1, FR3, FR2 and FR4.

to better comprehend the spectral response of the coupled system, Fig.2b–e shows the magnetic field distributions (H-field) $\lambda_{FR1} = 606$ nm, $\lambda_{FR2} = 842.1$ nm, $\lambda_{FR3} = 1142.8$ nm and $\lambda_{FR4} = 1702.1$ nm (from left to right peak). The resonance modes are classified by TM_m. Where m is the number of nodes of stationary waves in the defective oval resonator. From Fig. 2b–e apparently, the resonant modes are TM_6 , TM_4, TM_4,and TM_2, respectively. The contraction ratio of the resonant wavelentgh defined as $Tc = \frac{T_{max}}{T_{min}}$, where T_{max} is the maximal edge of the peak and T_{min} is the the lowest amount of the peak, is also a key parameter for practical applications. For the dips with wavelengths of 606 nm, 842.1 nm, 1142.8 nm and 1702.1 nm, the contraction ratios were determined as 16.75, 21.23, 12.47 and 114.59, respectively. Therefore, our proposed structure has a high contraction ratio, which is highly advantageous for operational usage in the same line, for the fourth fano resonance peak (TM2 mode), the electromagnetic wave energy was mainly confined in defective oval resonator. Therefore, this peak is more sensitive of the alteration of the refractive index around the surface of distribution, which is very helpful for enhancing the sensitivity and the performance of the biosensor.

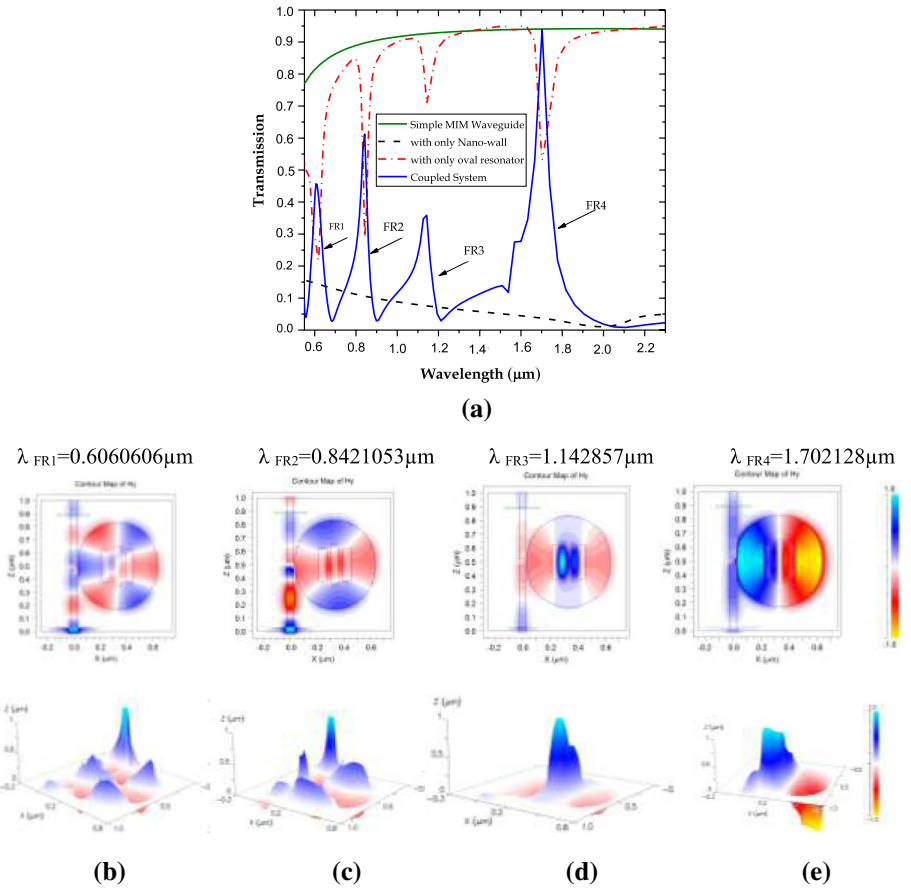

Fig. 2 **a** Transmission spectrum of the MIM waveguide, MIM waveguide with only Nano-wall, MIM waveguide with only defective oval resonator, and the coupled system (MIM waveguide with Nano-wall side-coupled to oval resonator) **b–e** Hy distribution of the coupled system with different resonance wavelength

The output characteristics transmission of the proposed structure were then studied with various values for some of the basic parameters. At the start, we keeped the previous parameters, and each time we analysed the transmission with the variation of a single parameter. The Fano resonances can be adjusted by the geometrical parameters of the metal nano-wall or the defective oval resonator. The effect of the thickness of the nano-wall D on the transmission spectra is studied and displayed in Fig. 3a. It is clear that the transmission decreases with increase of D. Since we are interested in studying the transmission of FR4 that has good confined electromagnetic field, we can obtain a good contraction ratio T_c and T_{max} when $D = 60$ nm (fig. 3b).

As shown in Fig. 3c, the increase of gap G from 10 to 30 nm can affect decrease the transmission spectrum. Additionally, It can be observed from Fig. 3d, the fano resonant wavelengths marked a very slight shift when the radius R of the defective oval increases from 280 to 320 nm. The reason is that for the given parameters, the increase the radius R of the oval can only slightly increase the effective length of the oval resonator. Moreover, the best performances with transmission value 0.94 were observed for FR4 at $R = 300$ nm.

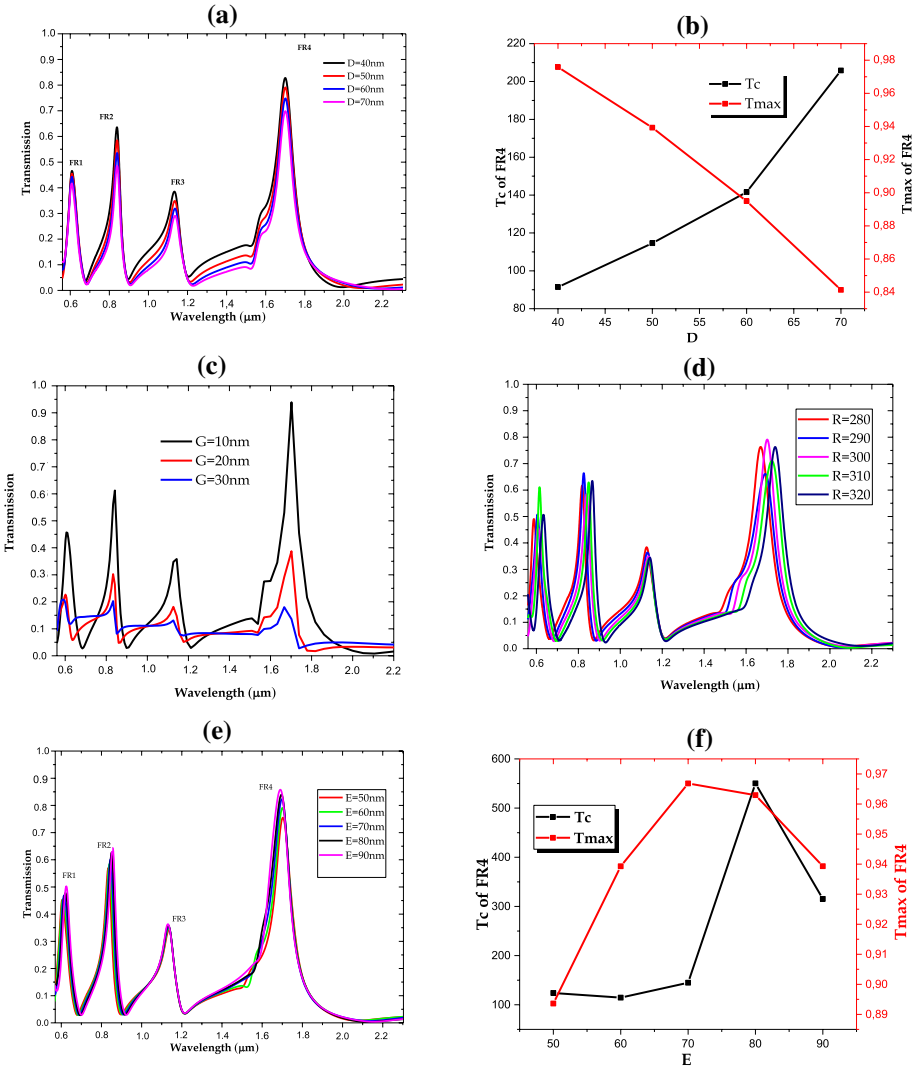

Fig. 3 **a** Transmission spectra with different thickness of the nano-wall D. **b** The contraction ratio T_c and the maximal edge T_{max} of the peak FR4 with different values of D. **c**, **d** and **e** transmission spectra with different gap G, radius R of defective oval and distance E between the two disks intertwined, respectively. **f** The contraction ratio T_c and the maximal edge T_{max} of the peak FR4 with different values of E,

To study the influence of the distance E between the two disks intertwined on the transmission characteristics, E is gradually increased from $E = 50$ nm to $E = 90$ nm . Fig.3e shows the transmission spectra for different values of E. It can be seen that as the distance E increases, the transmission increases, it reaches its maximum value for $E = 80$ nm and after that it decreases. Therefore, the best performances with transmission value of 0.96 and centration ratio 550.25 were observed for FR4 at $E = 80$ nm (Fig.3e).

The proposed structure can be employed in refractive index sensors, Owing to the extremely sensitive characteristics to different dielectric materials. the sensitivity (S) is

a vital parameter for sensors. It is characterized by the unit wavelength shift $\Delta\lambda$ of the unit RI change Δn (Wang et al. 2016; Zhang et al. 2016b), which can be expressed as $S = \frac{\Delta\lambda}{\Delta n}$. In addition to the sensitivity, the other term employed to evaluate the performance of a plasmonic sensor is the figure of merit (FOM), which can be expressed in terms of both the sensitivity (S) and the full width at half maximum (FWHM) of the resonance peak, $FOM = \frac{S}{(FWHM)}$ (Zhang et al. 2017).

As we mentioned before, the electromagnetic wave energy was mainly confined in defective oval resonator. Therefore, the peaks are sensitive of the alteration of the refractive index around the surface of distribution. By varying the refractive index of the defective oval from $n = 1$ to $n = 1.02$, can induce a shift of the resonance spectrum.

The sensing performance of the proposed structure was studied with various values of the defective resonator parameters. Furthermore, the effects of the geometric parameters on the sensitivity and FOM were analyzed to optimize the performance of the sensor (Fig. 4a, b, c). The sensitivity is calculated by varying RI of the oval resonator ($\Delta n = 0.02$). The effect of the distance Ds on sensitivity is studied (Fig. 4a). It is evident that only the peak FR3 is affected by the variation of the distance Ds from 20 to 40 nm, and for others peaks a very slight variation. The high sensitivity is obtainted with $Ds = 20\,\text{nm}$ and $30nm$. The relation between the sensitivity and the length of the lateral rectangle X is presented in Fig. 4b. Apparently, the high sensitivity is obtained for FR4 with $X = 400\,\text{nm}$ (Fig. 4b). The maximum $2.7 * 10^4$ of FOM, matching FR2 with $X = 300\,\text{nm}$ is calculated (Fig. 4c), which performs better than most other RI sensors (Zhang et al. 2017, 2018; Zhao and Yu 2018). In addition, the FOM of the peak FR4 that interests us and that has a high sensitivity varying from $9.78 * 10^3$ to $2.43 * 10^4$

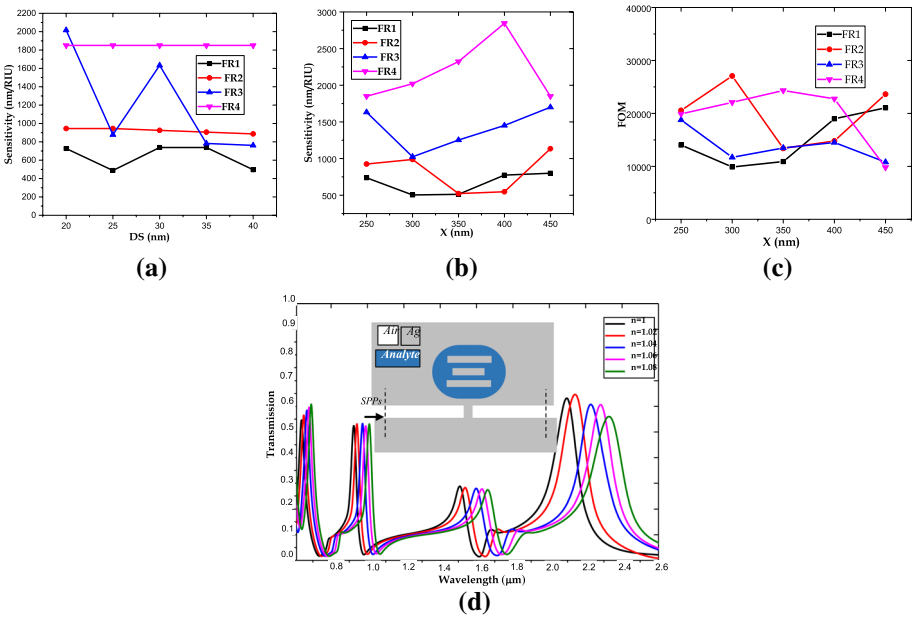

Fig. 4 **a** and **b** the sensitivity with different values of Ds and X, respectively. **c** The FOM with different values of X. **d** Transmission spectra for different n

when X varies from 250 nm to 450 nm. Finally, the transmission spectra of the optimal proposed design with different RI are presented in Fig. 4d.

3 Application prospect

Due to the extremely sharp line-shape, and dependency between the Fano peak wavelengths and the RI of the dielectric material, a high FOM and sensitivity of the spectral response can be given by the Fano resonance with varying the refractive index of the surrounding medium. By replacing the air in defective oval with ethanol whose refractive index is $n = 1.36084 - 3.94 * 10^{-4}(T - T_0)$, here $T_0 = 20°C$ (Wu et al. 2015), the designed structure can be served as an on-chip plasmonic temperature sensor.

The transmission spectrum is shown in Fig. 5a. As environmental temperature varies, the RI of the ethanol infiltrated in oval resonator change, which modulates spectral shapes and positions. High sensitive temperature measurements are recovered from the asymmetric spectral shape induced by the Fano resonance. With optimal parameters of the proposed design, the sensitivity temperature sensor is 2.463 nm/°C. Furthermore, according to linear fitting, the fano resonances wavelengths vary linearly with temperature variation as shown in Fig. 5b. Table 1 compares the sensitivity, for the proposed sensor with those obtained by other recently proposed devices, which shows that the proposed sensor has advantages in sensitivity.

4 Conclusion

In summary, four Fano resonant transmission spectra can be formed by a combined plasmonic structure made up of a MM waveguide with a thin nano-wall and a defective oval resonator. The coherent coupling and interference between the continua state which are supported by the waveguide with nano-wall and the four discrete states Which is generated by the defective oval resonator, generate the Fano resonance. FDTD-based numerical simulations are performed out to study the dependences of the geometry parameters on the

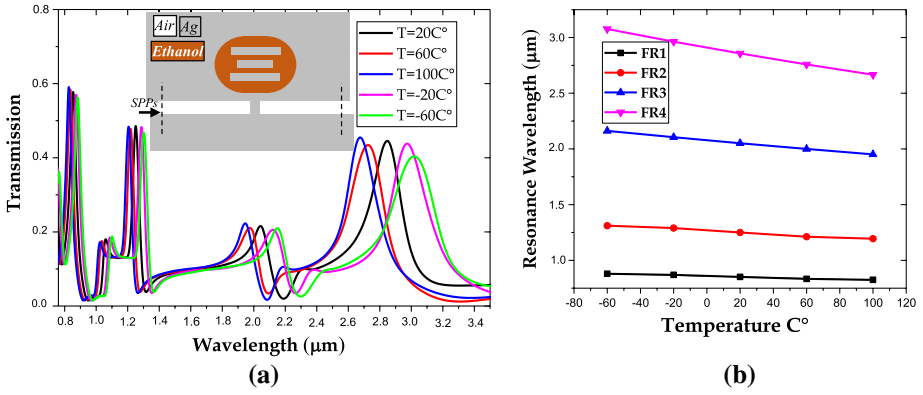

Fig. 5 **a** Transmission spectra with temperature variations. **b** Linear fitting between wavelengths of Fano resonances peak and temperature

Table 1 Sensitivity comparison of different sensor structures

Reference	Structure type	Wavelength (nm)	Sensitivity (nm/°C)
(Kong et al. 2017)	Rectangular resonator side coupled to MDM straight waveguide with a groove	1100–1350	0. 36
(Chen et al. 2019)	Ring resonator side coupled to MDM straight waveguide with a baffle	800–1400	0.31
(Tian et al. 2020)	Defective disk resonator side coupled to MDM straight waveguide with a baffle	1200–1700	0. 3925 for LFR and 0.4575 for RFR
(Yu et al. 2020)	MIM waveguide embodying a baffle and the coupled SSCDR inserted with a metallic block	600–2000	0.18 for FR3, 0.21for FR4 and 0.33 for FR6
This study	MIM waveguide with Nano-wall side-coupled to defective oval resonator	800–3200	0.44 for FR1, 0.94 forFR2, 1.282 for FR3. 2.46 for FR4

transmission properties. As one of the potential applications, i.e., the plasmonic RI sensor, the simulated results proved that the proposed sensor can achieve a high sensitivity and FOM, 2844. 95 nm/RIU and $2.27 * 10^4$ respectively corresponding to FR4 peak. In addition, another possible application is plasmonic temperature sensor, whose sensitivities are respectively 0.44 nm/°C, 0.94 nm/°C, 1.282 nm/°C and 2.46 nm/°C corresponding to FR1, FR2, FR3 and FR4. Finally, this design due to its small size , high sensitivity and high value of FoM, is very suitable for use in highly integrated circuits..

Acknowledgements This work was supported by the Algerian Ministry of Higher Education and Scientific Research and La Direction Générale de la Recherche Scientifique et du Développement Technologique (DGRSDT) via funding through the PRFU Project No. A25N01UN28012 0180001.

References

Achi, S.E., Hocini, A., Salah, H.B., Harhouz, A.: Refractive index sensor MIM based waveguide coupled with a slotted side resonator. Progress Electromagn. Res. **96**, 147–156 (2020)

Barnes, W.L., Dereux, A., Ebbesen, T.W.: Surface plasmon subwavelength optics. Nature **424**(6950), 824–830 (2003)

Bashiri, J., Rezaei, B., Barvestani, J., Zapata-Rodríguez, C.: Bloch surface waves engineering in one-dimensional photonic crystals with a chiral cap layer. JOSA B **36**(8), 2106–2113 (2019)

Bensalah, H., Hocini, A., Temmar, M., Khedrouche, D., et al.: Design of mid infrared high sensitive metal-insulator-metal plasmonic sensor. Chin. J. Phys. **61**, 86–97 (2019)

Binfeng, Y., Hu, G., Zhang, R., Yiping, C.: Fano resonances in a plasmonic waveguide system composed of stub coupled with a square cavity resonator. J. Opt. **18**(5), 055002 (2016)

Chatterjee, S., Palermo, G., Letsou, T., Lio, G., De Luca, A., Strangi, G.: Temperature and refractive index sensing based on plasmonic fano resonance, Proceedings of the 3 rd International Conference of Theoretical and Applied Nanoscience and Nanotechnology (TANN'19) Ottawa, Canada – June (2019)

Chen, F., Zhang, H., Sun, L., Li, J., Yu, C.: Temperature tunable fano resonance based on ring resonator side coupled with a mim waveguide. Opt. Laser Technol. **116**, 293–299 (2019)
Chen, Z., Yu, L., Wang, L., Duan, G., Zhao, Y., Xiao, J.: Sharp asymmetric line shapes in a plasmonic waveguide system and its application in nanosensor. J. Lightwave Technol. **33**(15), 3250–3253 (2015)
Danaie, M., Shahzadi, A.: Design of a high-resolution metal-insulator-metal plasmonic refractive index sensor based on a ring-shaped si resonator. Plasmonics **14**(6), 1453–1465 (2019)
Dong, L., Xu, X., Li, C., Guo, Y., Sun, K., Ding, Y.: Plasmon-induced transparency in sensing application with semicircle cavity waveguide. Opt. Commun. **410**, 751–755 (2018)
Gai, H., Wang, J., Tian, Q.: Modified debye model parameters of metals applicable for broadband calculations. Appl. Opt. **46**(12), 2229–2233 (2007)
Ghorbani, S., Dashti, M.A., Jabbari, M.: Plasmonic nano-sensor based on metal-dielectric-metal waveguide with the octagonal cavity ring. Laser Phys. **28**(6), 066208 (2018)
Goyal, A.K., Pal, S.: Design analysis of bloch surface wave based sensor for haemoglobin concentration measurement. Appl. Nanosci. **10**, 3639–3647 (2020)
Goyal, A.K., Saini, J.: Performance analysis of bloch surface wave-based sensor using transition metal dichalcogenides. Appl. Nanosci. **10**(11), 4307–4313 (2020)
Hocini, A., Khedrouche, D., Melouki, N., et al.: A high-sensitive sensor and band-stop filter based on intersected double ring resonators in metal-insulator-metal structure. Opt. Quant. Electron. **52**(7), 1–10 (2020)
Hocini, A., Ben Salah, H. & Temmar, M.N.: Ultra-high-sensitive sensor based on a metal–insulator–metal waveguide coupled with cross cavity. J. Comput. Electron. **20**, 1354–1362 (2021)
Kong, Y., Qiu, P., Wei, Q., Quan, W., Wang, S., Qian, W.: Refractive index and temperature nanosensor with plasmonic waveguide system. Opt. Commun. **371**, 132–137 (2016)
Kong, Y., Wei, Q., Liu, C., Wang, S.: Nanoscale temperature sensor based on fano resonance in metal-insulator-metal waveguide. Opt. Commun. **384**, 85–88 (2017)
Li, Q., Wang, T., Su, Y., Yan, M., Qiu, M.: Coupled mode theory analysis of mode-splitting in coupled cavity system. Opt. Express **18**(8), 8367–8382 (2010)
Lin, G., Yang, H., Deng, Y., Wu, D., Zhou, X., Wu, Y., Cao, G., Chen, J., Sun, W., Zhou, R.: Ultra-compact high-sensitivity plasmonic sensor based on fano resonance with symmetry breaking ring cavity. Opt. Express **27**(23), 33359–33368 (2019)
Liu, N., Weiss, T., Mesch, M., Langguth, L., Eigenthaler, U., Hirscher, M., Sonnichsen, C., Giessen, H.: Planar metamaterial analogue of electromagnetically induced transparency for plasmonic sensing. Nano Lett. **10**(4), 1103–1107 (2010)
Lu, H., Liu, X., Mao, D., Gong, Y., Wang, G.: Induced transparency in nanoscale plasmonic resonator systems. Opt. Lett. **36**(16), 3233–3235 (2011)
MacDonald, K.F., Sámson, Z.L., Stockman, M.I., Zheludev, N.I.: Ultrafast active plasmonics. Nat. Photonics **3**(1), 55–58 (2009)
Ozbay, E.: Plasmonics: merging photonics and electronics at nanoscale dimensions. Science **311**(5758),189–193 (2006)
Piao, X., Yu, S., Koo, S., Lee, K., Park, N.: Fano-type spectral asymmetry and its control for plasmonic metal-insulator-metal stub structures. Opt. Express **19**(11), 10907–10912 (2011)
Piao, X., Yu, S., Park, N.: Control of fano asymmetry in plasmon induced transparency and its application to plasmonic waveguide modulator. Opt. Express **20**(17), 18994–18999 (2012)
Tang, Y., Zhang, Z., Wang, R., Hai, Z., Xue, C., Zhang, W., Yan, S.: Refractive index sensor based on fano resonances in metal-insulator-metal waveguides coupled with resonators. Sensors **17**(4), 784 (2017)
Tian, J., Wei, G., Yang, R., Pei, W.: Fano resonance and its application using a defective disk resonator coupled to an mdm plasmon waveguide with a nano-wall. Optik **208**, 164136 (2020)
Tong, L., Wei, H., Zhang, S., Xu, H.: Recent advances in plasmonic sensors. Sensors **14**(5), 7959–7973 (2014)
Wang, M., Zhang, M., Wang, Y., Zhao, R., Yan, S.: Fano resonance in an asymmetric mim waveguide structure and its application in a refractive index nanosensor. Sensors **19**(4), 791 (2019)
Wang, R., Xia, H., Zhang, D., Chen, J., Zhu, L., Wang, Y., Yang, E., Zang, T., Wen, X., Zou, G., et al.: Bloch surface waves confined in one dimension with a single polymeric nanofibre. Nat. Commun. **8**(1), 1–10 (2017)
Wang, Y., Li, S., Zhang, Y., Yu, L.: Ultrasharp fano resonances based on the circular cavity optimized by a metallic nanodisk. IEEE Photonics J. **8**(6), 1–8 (2016)
Wen, K., Hu, Y., Chen, L., Zhou, J., Lei, L., Guo, Z.: Fano resonance with ultra-high figure of merits based on plasmonic metal-insulator-metal waveguide. Plasmonics **10**(1), 27–32 (2015)

Wen, K., Yan, L., Pan, W., Luo, B., Guo, Z., Guo, Y., Luo, X.: Electromagnetically induced transparency-like transmission in a compact side-coupled t-shaped resonator. J. Lightwave Technol. **32**(9), 1701–1707 (2014)

Wu, T., Liu, Y., Yu, Z., Ye, H., Peng, Y., Shu, C., Yang, C., Zhang, W., He, H.: A nanometeric temperature sensor based on plasmonic waveguide with an ethanol-sealed rectangular cavity. Optics Communications **339**, 1–6 (2015)

Yan, S.-B., Luo, L., Xue, C.-Y., Zhang, Z.-D.: A refractive index sensor based on a metal-insulator-metal waveguide-coupled ring resonator. Sensors **15**(11), 29183–29191 (2015)

Yin, Y., Qiu, T., Li, J., Chu, P.K.: Plasmonic nano-lasers. Nano Energy **1**(1), 25–41 (2012)

Yu, S., Piao, X., Hong, J., Park, N.: Progress toward high-q perfect absorption: a fano antilaser. Phys. Rev. A **92**(1), 011802 (2015)

Yu, S., Wang, S., Zhao, T., Yu, J.: Tunable plasmonic system based on a slotted side-coupled disk resonator and its multiple applications on chip-scale devices. Optik, pp. 164748 (2020)

Yu, S., Zhao, T., Yu, J., Pan, D.: Tuning multiple fano resonances for on-chip sensors in a plasmonic system. Sensors **19**(7), 1559 (2019)

Zayats, A.V., Smolyaninov, I.I., Maradudin, A.A.: Nano-optics of surface plasmon polaritons. Phys. Rep. **408**(3–4), 131–314 (2005)

Zhang, X., Qi, Y., Zhou, P., Gong, H., Hu, B., Yan, C.: Refractive index sensor based on fano resonances in plasmonic waveguide with dual side-coupled ring resonators. Photonic Sensors **8**(4), 367–374 (2018)

Zhang, X., Shao, M., Zeng, X.: High quality plasmonic sensors based on fano resonances created through cascading double asymmetric cavities. Sensors **16**(10), 1730 (2016a)

Zhang, Y., Li, S., Chen, Z., Jiang, P., Jiao, R., Zhang, Y., Wang, L., Yu, L.: Ultra-high sensitivity plasmonic nanosensor based on multiple fano resonance in the mdm side-coupled cavities. Plasmonics **12**(4), 1099–1105 (2017)

Zhang, Y., Li, S., Zhang, X., Chen, Y., Wang, L., Zhang, Y., Yu, L.: Evolution of fano resonance based on symmetric/asymmetric plasmonic waveguide system and its application in nanosensor. Opt. Commun. **370**, 203–208 (2016b)

Zhao, T., Yu, S.: Ultra-high sensitivity nanosensor based on multiple fano resonance in the mim coupled plasmonic resonator. Plasmonics **13**(4), 1115–1120 (2018)

Zhou, N., Ye, C., Polavarapu, L., Xu, Q.-H.: Controlled preparation of au/ag/sno 2 core-shell nanoparticles using a photochemical method and applications in lspr based sensing. Nanoscale **7**(19), 9025–9032 (2015)